Laser and Particle Beams (2017), *35*, 58–63.

doi:10.1017/S0263034616000811

Plasma scale length effects on protons generated in ultra-intense laser–plasmas

O. CULFA,[1,2,3] G.J. TALLENTS,[3] M.E. KORKMAZ,[1] A.K. ROSSALL,[3] E. WAGENAARS,[3] C.P. RIDGERS,[3] C.D. MURPHY,[3] N. BOOTH,[4] D.C. CARROLL,[4] L.A. WILSON,[4] K.L. LANCASTER,[3,4] AND N.C. WOOLSEY[3]

[1]Department of Physics, Karamanoglu MehmetBey University, Karaman, Turkey
[2]Horia Hulubei National Institute of Physics & Nuclear Engineering, IFIN-HH, ELI NP, Magurele, Romania
[3]Department of Physics, York Plasma Institute, The University of York, York, YO10 5DD, UK
[4]CLF, STFC Rutherford Appleton Laboratory, Didcot, Oxfordshire OX11 0QX, UK

(RECEIVED 5 September 2016; ACCEPTED 12 November 2016)

Abstract

The energy spectra of protons generated by ultra-intense (10^{20} W cm^{-2}) laser interactions with a preformed plasma of scale length measured by shadowgraphy are presented. The effects of the preformed plasma on the proton beam temperature and the number of protons are evaluated. Two-dimensional EPOCH particle-in-cell code simulations of the proton spectra are found to be in agreement with measurements over a range of experimental parameters.

Keywords: High-power lasers; Laser–plasma interactions; Proton acceleration

1. INTRODUCTION

High-power lasers are enabling the irradiation of solid targets at irradiances exceeding 10^{18} W cm^{-2} with consequent production of high-energy electrons, ions, and X rays. Experiments have demonstrated intense bursts of ions emitted from the rear of targets (the non-irradiated side) with energies up to several tens of mega-electron volts (Daido *et al.*, 2012; Macchi *et al.*, 2013) with the acceleration produced by the production of an electric potential sheath associated with fast electrons penetrating through the target. The planar nature of targets enables an approximately one-dimensional (1D) acceleration of ions with the process referred to as target normal sheath acceleration (TNSA). Protons arising from impurity hydrogen on the back surface of the targets are preferentially accelerated due to their high charge-to-mass ratio compared with other ions and their abundance in typical targets at the surface.

The physics of TNSA as an explanation of energetic protons emitted from the back of solid targets during Petawatt-laser irradiation was first presented by Wilks *et al.* (2001) following the experimental evidence of Mackinnon *et al.* (2001) that the protons are accelerated at the back rather than the front of the target. More recent results have been reviewed by Roth and Schollmeier (2016). The irradiance of 10^{18} W cm^{-2} for laser light of wavelength λ about 1 μm represents the threshold for the $\mathbf{J}\times\mathbf{B}$ electron acceleration process to become significant. In $\mathbf{J}\times\mathbf{B}$ acceleration, electrons are accelerated in the direction of the laser **k**-vector due to a $\mathbf{J}\times\mathbf{B}$ force arising from a transverse current $\mathbf{B} = n_e e\mathbf{E}$, where **E** and **B** are the laser electric and magnetic fields, respectively, and n_e is the electron density. The $\mathbf{J}\times\mathbf{B}$ acceleration starts to dominate at irradiances $>10^{18}$ W cm^{-2} where the ponderomotive potential ($e^2E_o^2/4m\omega^2$ with $\omega = 2\pi c/\lambda$) exceeds the electron rest mass energy (mc^2). At irradiances $>10^{18}$ W cm^{-2}, electrons are accelerated to relativistic velocities into the target. Due to the low cross-section for relativistic electron collisions with atoms, the electrons pass through even thick (>10 μm) targets, with current flow limited by the Alfven limit as moderated by a return current from back to front of the target. Alfven showed that the limiting factor for the propagation of an electron beam is the self-generated magnetic beam, which bends the electrons back toward their source (Alfven, 1939). A return current in the irradiated target area enables the Alfven limit for the electron flux to be exceeded and a potential in electron volts at the back of the target of value equal to the hot electron temperature T_e in electron volts to be formed (Wilks *et al.*, 2001).

The propagation and application of laser-accelerated electrons passing through the solid target are a subject of ongoing research. For example, there is evidence associated with hollow ion emission for the creation of intense radiation

Address correspondence and reprint requests to: O. Culfa, Department of Physics, Karamanoglu MehmetBey University, Karaman, Turkey. E-mail: ozgurculfa@kmu.edu.tr

fields equivalent to keV blackbody intensities due to electrons undergoing bremsstrahlung and Thomson scattering as they propagate through the target (Colgan *et al.*, 2013; Hansen *et al.*, 2013). In hollow ions, two or more bound electrons are removed from an atomic inner shell giving rise to uniquely identifiable spectral lines. Such double ionization from an inner shell can only be produced by an intense radiation field as Auger processes quickly fill vacant inner-shell quantum states and, if significant, collisional ionization is closely balanced by collisional three-body recombination.

Experimental parameter studies showing the effects of target thickness and the plasma scale length at the front of the target are useful in elucidating understanding and in the development of applications of laser-accelerated protons arising from the back of the target. We present measurements of the energies of protons accelerated from the rear of targets along the target normal in ultra-intense irradiation at 10^{20} W cm^{-2}. We have deliberately used a pre-pulse to irradiate the target before the high-power laser irradiation in order to establish a plasma of controlled scale length into which the high-power laser interacts. The scale length of the plasma formed by the pre-pulse at the time of the high-power laser irradiance is measured using transverse probe shadowgraphy. Electron energy and temperature measurements with the controlled density scale length have been reported by Culfa *et al.* (2016, 2014). This paper investigates the effects of the electrons accelerated through the target on the TNSA of protons measured along the target normal at the back of the target. We present ion spectra and fitted temperatures as a function of the plasma density scale length and target thickness. Our experimental measurements are consistent with 2D particle-in-cell (PIC) code simulations also presented.

2. EXPERIMENTAL SETUP

The Vulcan laser system at the Rutherford Appleton Laboratory (RAL) has been utilized for the measurement of proton energies. The petawatt-laser delivers 1.054 μm wavelength laser pulses of ~1 ps duration and pulse energies 150 ± 20 J with an intensity contrast of 10^8. Laser irradiance of 10^{20} W cm^{-2} in a p-polarized beam was an incident at 40° angle to a plane target normal. A 5 ns duration pre-pulse was an incident at 17° incidence angle with peak irradiance 1.5 ns prior to the main pulse. The petawatt laser was focused onto plane foil of parylene-N (CH) in various thicknesses from 6 to 150 μm. The targets contained a thin (100 nm) layer of aluminum buried at depths ≥3 μm from the target surface. The experimental setup is schematically illustrated in Figure 1.

A frequency doubled optical probe beam was used to record the expanding density profile of the plasma at the time of the interaction pulse. The probe beam was directed parallel to the target surface passing through the plasma produced by the longer pulse laser–target interaction. In our previous work (Culfa *et al.*, 2016), we have discussed in detail how to measure and analyze plasma density scale length from the shadowgraphy images obtained using the optical probe.

The distribution of multi-MeV protons along the target normal from the rear of the target were measured as a function of energy using passive stacks of dosimetry radiochromic film (RCF) (Nurnberg *et al.*, 2009), which were located 5 cm from the rear of the target and centered on the target normal axis. Number, energy, and fitted temperature of accelerated protons were measured as a function of target thickness and the plasma scale length, which varies with the pre-pulse intensity (Culfa *et al.*, 2014).

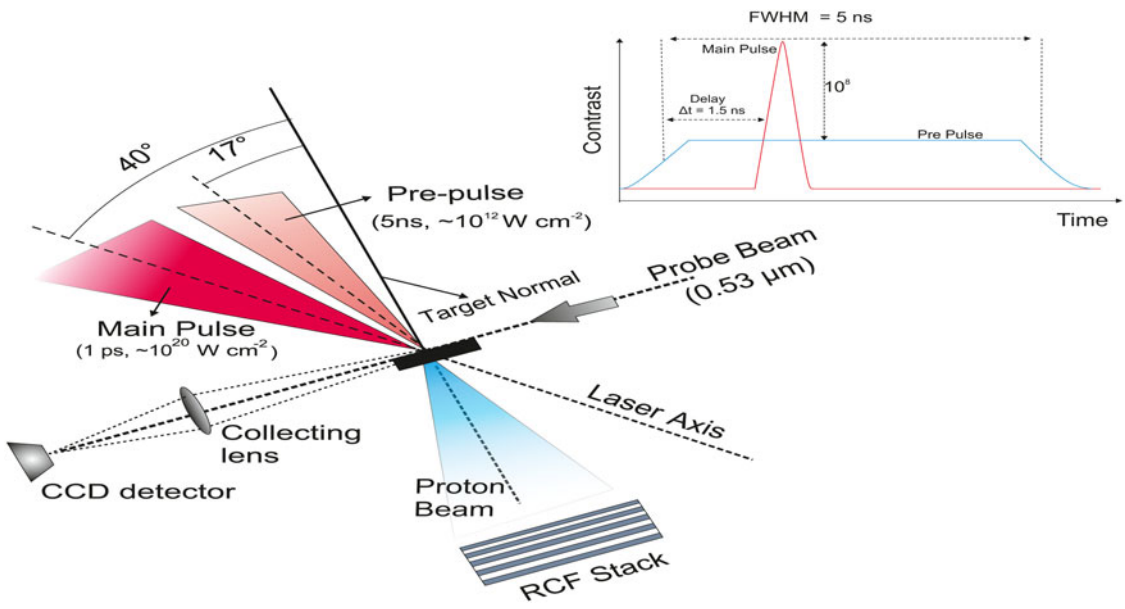

Fig. 1. Experimental setup in the Vulcan Petawatt Laser Facility for the measurement of proton energy along the target normal and density gradients normal to the target surface. The inset shows the timing of a pre-pulse used to modify the interaction density scale length.

https://doi.org/10.1017/S0263034616000811 Published online by Cambridge University Press

3. EXPERIMENTAL RESULTS

Proton numbers as a function of energy have been deduced from stacked RCF (Gafchromic HDF-810) exposure. A 10 μm thick aluminum foil acts to block scattered laser light and all plasma thermal emissions expected from the back of the target (photon energies < 1 keV). The electron flux of energy up to 200 MeV is directed parallel to the laser axis at 40° to the target normal (Culfa *et al.*, 2016) and is not directed at the RCF stack. Protons are attenuated in the RCF stack of RCFs as they transmit through the different films and interspersed filters, with the exposure of the films giving the flux of protons of energy sufficient to penetrate through the overlay films and filters. Each film exposes predominantly at a particular proton energy due to the Bragg peak nature of proton absorption in matter. The background angle independent exposure of the RCF film includes exposure due to hard X-ray emission (>1 keV) and is subtracted from exposure measurements. More details of the RCF measurements of proton energies and the method of analysis are given by Schollmeier *et al.* (2014).

Proton numbers recorded from the back of the target were found to peak on the target normal axis consistent with TNSA acceleration. The log-linear nature of the proton energy spectra allows a deduction of a proton temperature (kT_p) by fitting the proton spectra with variations of form exp $(-E/kT_p)$. The variation of the fitted temperatures with the target thickness and the measured front surface density scale length are shown in Figures 2 and 3, respectively.

The total number N_T of protons can be evaluated from the proton energy spectra using the spectrum number in MeV extrapolated to zero energy ($n(0)$) and multiplying by the deduced proton temperature. We can write that

$$N_T = \int_0^\infty n(0)\exp\left(\frac{-E}{kT_p}\right)dE = n(0)kT_p. \quad (1)$$

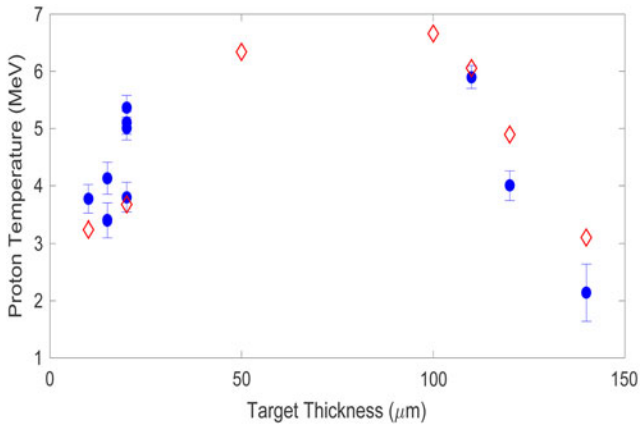

Fig. 2. Experimental and simulated measurements of proton temperature as a function of the target thickness for a number of individual laser shots. The plasma density scale length measured experimentally and used in the simulation was fixed at 0.5 μm. Red diamonds represent the PIC code simulations and blue circles are the experimental data

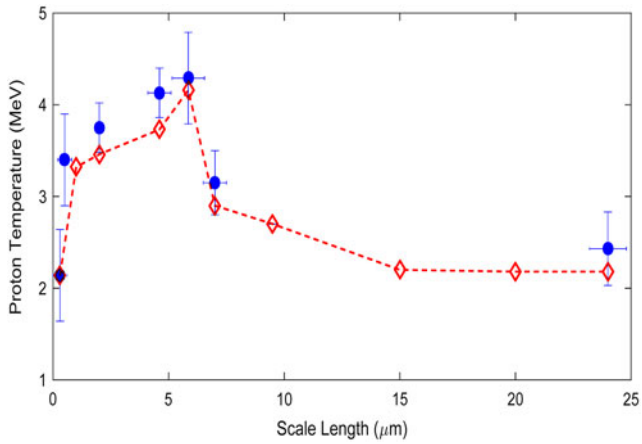

Fig. 3. Experimental measurements of proton temperature as a function of the measured plasma density scale length for a number of individual laser shots (circles) with target thickness of 20 μm. Superimposed are 2D PIC code simulations (red diamonds) with the preformed scale length and experimental parameters of the experiment.

The number of fast electrons increases with the density scale length (Culfa *et al.*, 2014) and this results in a larger number of protons with increasing scale length (Fig. 4).

4. COMPARISON OF EPOCH 2D PIC CODE SIMULATIONS WITH EXPERIMENTALLY MEASURED PROTON SPECTRA

The 2D PIC code EPOCH (Arber *et al.*, 2015) was used to simulate the experimental proton spectra for different target thicknesses and plasma density scale length. The system size was 90×90 μm^2 with a mesh resolution of 1000×1000 cells with 48 particles of electrons and protons in a cell. The experimental variation of proton energy spectra for different target thicknesses with the laser irradiance of 3.5×10^{20} W cm^{-2} focused on a 7 μm focal spot with an incidence angle of 40° was determined. The laser wavelength

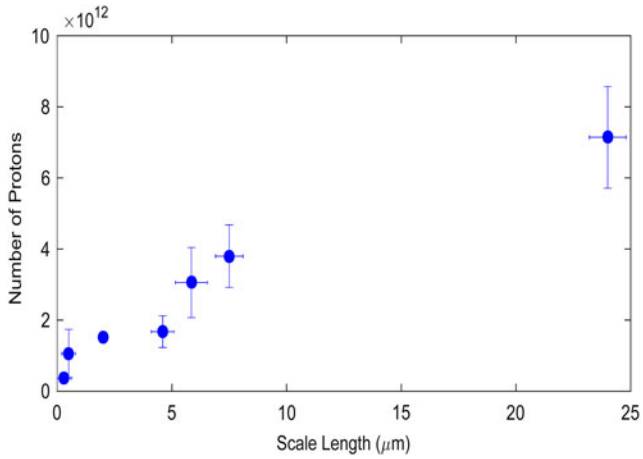

Fig. 4. Experimental measurements of a number of protons as a function of the measured plasma scale length for a number of individual laser shots.

https://doi.org/10.1017/S0263034616000811 Published online by Cambridge University Press

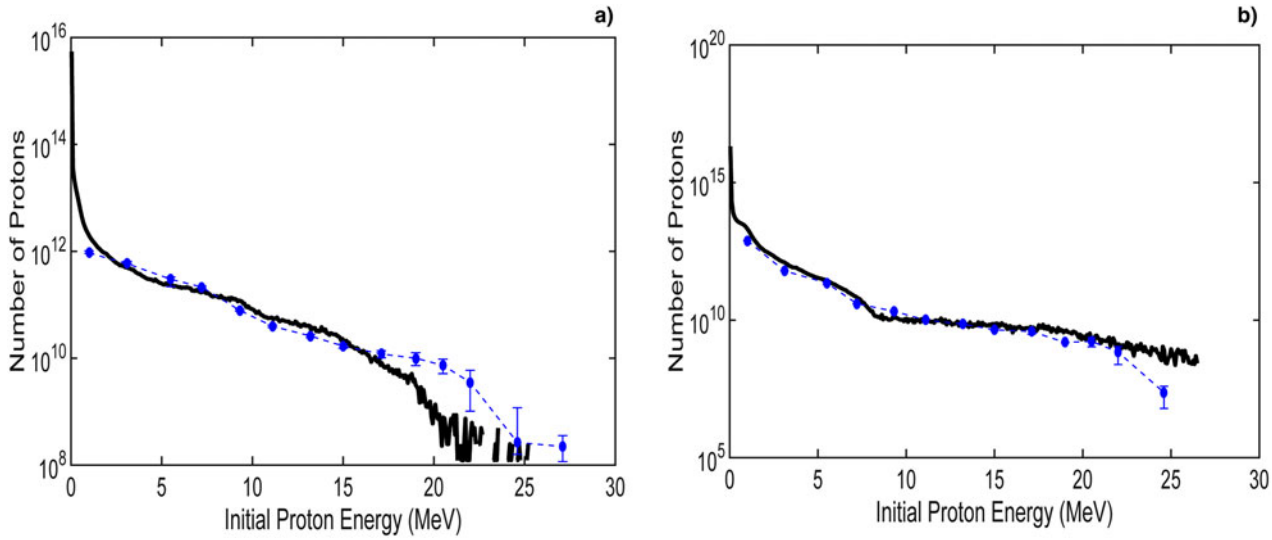

Fig. 5. Comparison of EPOCH 2D PIC code results with experimental proton spectra for (a) 20 μm, (b) 120 μm target thickness. The continuous black line represents the simulation results, while the blue dotted points are the experimental data. The absolute values of vertical scales are arbitrary and the experimental and simulated spectra are visually superimposed to match vertically.

and pulse duration were 1 μm and 1 ps, respectively. In the simulations, the peak electron density was limited at $50n_c$, where n_c is the critical density. A constant exponential density profile was assumed with the scale lengths L in the range of 0.5–25 μm.

The proton energy spectra was extracted at time 0.5 ps. Figure 5 compares the generated proton spectra from the 2D PIC code to the experimental proton energy spectra for different target thicknesses. The continuous line represents the EPOCH 2D PIC code simulation results and red dotted line with diamonds shows our experimental observations.

In order to understand the increase in the number of protons with increasing scale length with a constant target thickness block (20 μm thick). We present simulation results for the TNSA sheath field with varying scale length and target thickness (Figs. 6 and 7).

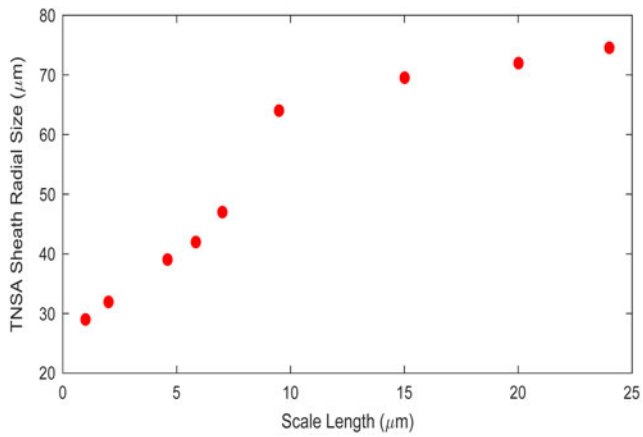

Fig. 6. Simulation results for TNSA sheath field measurements as a function of the plasma scale length.

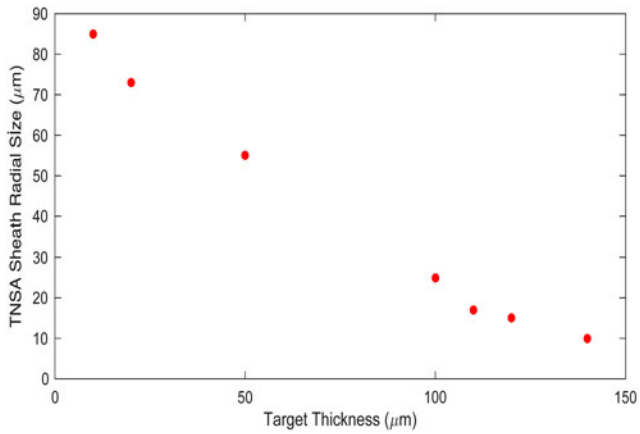

Fig. 7. Measured TNSA sheath field distance obtained by EPOCH 2D PIC simulations as a function of the target thickness

Experimentally measured and simulated results of proton temperature as a function of the target thickness can be seen in Figure 2 and as a function of plasma scale length in Figure 3. Blue circles represent the experimental results, while red diamonds represent PIC simulations. Experimental and simulation results show that peak proton temperature occurs for target thickness about 50 μm and density scale lengths about 5 μm.

At the high irradiances (10^{20} W cm^{-2}) of our experiment, electrons are expelled from the laser propagation axis due to the ponderomotive force. The plasma refractive index on axis is increased due to the electron density drop which produces a positive lensing effect (Max *et al.*, 1974). Laser pulses also undergo self-focusing due to the relativistic mass increase of the electrons accelerated by high-irradiance laser light (Naseri *et al.*, 2010). The transverse ponderomotive force can be sufficiently large to expel a significant fraction of

https://doi.org/10.1017/S0263034616000811 Published online by Cambridge University Press

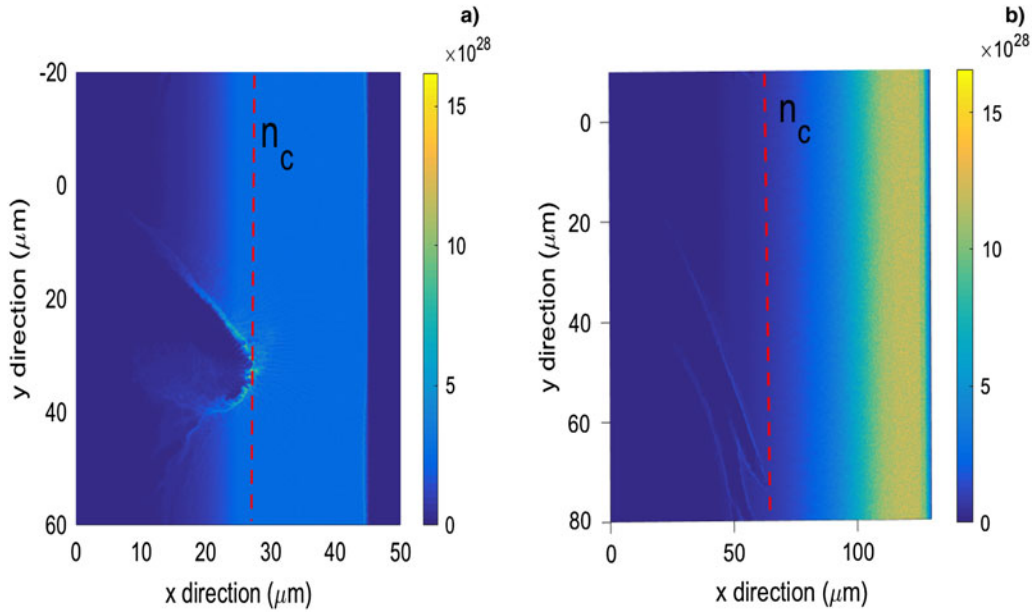

Fig. 8. An example of electron density values color-coded in units of m^{-3} after 0.55 ps with (a) 5 μm, (b) 15 μm scale length as simulatzed by the EPOCH 2D PIC code. The dashed vertical line indicates the critical density surface. The laser radiation is incident at 40° to the target normal.

the electrons from the high-intensity laser region creating ion channels (see Fig. 8). With the longer plasma propagation distances associated with longer plasma scale lengths, the laser pulse can be subject to transverse instabilities, resulting in beam filamentation. The filamentation reduces the local laser irradiance and reduces the temperature of accelerated electrons (Culfa *et al.*, 2016). The drop in electron temperature reduces the generated proton temperature as well at the longer scale lengths. The measured proton temperatures vary with plasma scale length (Fig. 3) following the electron temperature, which show a peak at scale lengths of 7.5 μm (see Culfa *et al.*, 2016).

5. CONCLUSION

We have presented measurements of number, energy, and temperature of protons in high-irradiance laser–plasma interactions with a preformed plasma of measured density scale length. The experimentally observed proton temperatures decrease for longer scale lengths as predicted by a 2D PIC code. Our experimental and simulation parameter studies of proton energies from high-irradiance laser plasmas show that the 2D PIC code simulations are accurate and will help in the development of applications for laser-accelerated protons.

ACKNOWLEDGMENTS

The authors gratefully acknowledge the assistance of laser operations, target preparation and engineering staff at the Central Laser Facility of RAL. Part of the research was supported by Karamanoglu Mehmetbey University Research Project 37-M-16. This work was in part funded by the UK EPSRC grants EP/G054950/1, EP/G056803/1, EP/G055165/1, and EP/M022463/1.

REFERENCES

Alfven, H. (1939). On the motion of cosmic rays in interstellar space. *Phys. Rev*. **55**, p. 425.

Arber, T.D., Bennett, K., Brady, C.S., Lawrence-Douglas, A., Ramsay, M.G., Sircombe, N.J., Gillies, P., Evans, R.G., Schmitz, H., Bell, A.R. & Ridgers, C.P. (2015). Contemporary particle-in-cell approach to laser-plasma modelling. *Plasma Phys. Control. Fusion* **57**, pp. 1–26.

Colgan, J., Abdallah, J., Faenov, A.Y., Pikuz, S.A., Wagenaars, E., Booth, N., Culfa, O., Dance, R.J., Evans, R.G., Gray, R.J., Kaempfer, T., Lancaster, K.L., McKenna, P., Rossall, A.L., Skobelev, I.Y., Schulze, K.S., Uschmann, I., Zhidkov, A.G. & Woolsey, N.C. (2013). Exotic dense-matter states pumped by a relativistic laser plasma in the radiation-dominated regime. *Phys. Rev. Lett*. **110**, p. 125001.

Culfa, O., Tallents, G.J., Rossall, A.K., Wagenaars, E., Ridgers, C.P., Murphy, C., Dance, R.J., Gray, R.J., McKenna, P., Brown, C.D.R., James, S.F., Hoarty, D.J., Booth, N., Robinson, A.P.L., Lancaster, K.L., Pikuz, S.A., Faenov, A.Y., Kampfer, T., Schulze, K.S., Uschmann, I. & Woolsey, N.C. (2016). Plasma scale-length effects on electron energy spectra in high-irradiance laser plasmas. *Phys. Rev. E* **93**, p. 043201

Culfa, O., Tallents, G.J., Wagenaars, E., Ridgers, C.P., Dance, R.J., Rossall, A.K., Gray, R.J., McKenna, P., Brown, C.D.R., James, S.F., Hoarty, D.J., Booth, N., Robinson, A.P.L., Lancaster, K.L., Pikuz, S.A., Faenov, A.Y., Kampfer, T., Schulze, K.S., Uschmann, I. & Woolsey, N.C. (2014). Hot electron production in laser solid interactions with a controlled pre-pulse. *Phys. Plasmas* **21**, pp. 043106

https://doi.org/10.1017/S0263034616000811 Published online by Cambridge University Press

Daido, H., Nishiuchi, M. & Pirozhkov, A. (2012). Review of laser-driven ion sources and their applications. *Rep. Prog. Phys*. **75**, p. 056401

Hansen, S.B., Colgan, J., Faenov, A.Y., Abdallah, J., Pikuz, S.A., Skobelev, I.Y., Wagenaars, E., Booth, N., Culfa, O., Dance, R.J., Tallents, G.J., Evans, R.G., Gray, R.J., Kaempfer, T., Lancaster, K.L., McKenna, P., Rossall, A.K., Schulze, K.S., Uschmann, I., Zhidkov, A.G. & Woolsey, N.C. (2013). Detailed analysis of hollow ions spectra from dense matter pumped by x-ray emission of relativistic laser plasma. *Phys. Plasmas* **21**, p. 031213

Macchi, A., Borghesi, M. & Passoni, M. (2013). Ion acceleration by super intense laser–plasma interaction. *Rev. Mod. Phys*. **85**, pp. 751–793.

Mackinnon, A.J., Borghesi, M., Hatchett, S., Key, M.H., Patel, P.K., Campbell, H., Schiavi, A., Snavely, R., Wilks, S.C. & Willi, O. (2001). Effect of plasma scale Length on multi-MeV proton production by intense laser pulses. *Phys. Rev. Lett*. **86**, pp. 1769–1772.

Max, C., Arons, J. & Langdon, A. (1974). Self-modulation and self-focusing of electromagnetic waves in plasmas. *Phys. Rev. Lett*. **33**, p. 209

Naseri, N., Bochkarev, S.G. & Rozmus, W. (2010). Self-channelling of relativistic laser pulses in large-scale underdense plasmas. *Phys. Plasmas* **17**, p. 033107

Nurnberg, F., Schollmeier, M., Brambrink, E., Blazevic, A., Carroll, D.C., Flippo, K., Gautier, D.C., Geibel, M., Harres, K., Hegelich, B.M., Lundh, O., Markey, K., McKenna, P., Neely, D., Schreiber, J. & Roth, M. (2009). Radiochromic film imaging spectroscopy of laser-accelerated proton beams. *Rev. Sci. Inst*. **80**, p. 033301

Roth, M. & Schollmeier, M. (2016). Ion acceleration—target normal sheath acceleration. *CERN Yellow Rep*. **1**, p. 231

Schollmeier, M., Geissel, M., Sefkow, A.B. & Flippo, K.A. (2014). Improved spectral data unfolding for radiochromic film imaging spectroscopy of laser-accelerated proton beams. *Rev. Sci. Inst*. **85**, p. 043305

Wilks, S., Langdon, A., Cowan, T., Rooth, M., Singh, M., Hatchett, S., Key, M., Pennington, D., MacKinnon, A. & Snavely, R. (2001). Energetic proton generation in ultra-intense laser–solid interactions. *Phys. Plasmas* **8**, pp. 542–549..

https://doi.org/10.1017/S0263034616000811 Published online by Cambridge University Press